Miniaturized Enzyme-Based glucose / O_2 Fuel Cell Using Vitamin K3 as Electron Mediator

F. Sato[1], M. Togo[1], T. Abe[1], T. Ohashi[2], I. M. Kamrul[2],
T. Matsue[2], J. Kosuge[3], N. Fukasaku[3], and M. Nishizawa[1]

[1]Department of Bioengineering and Robotics, [2]Department of Biomolecular Chemistry,
Graduate School of Engineering, Tohoku University,
Aoba 6-6-01, Aramaki, Aoba- ku, Sendai, Miyagi 980-8579, Japan
Tel +81-22-217-7003, Fax +81-22-217-3586, nishizawa@biomems.mech.tohoku.ac.jp
[3]Daiichi Pure Chemicals Co., Ltd.
Matsumura 2117, Tokai, Naka, Ibaraki 319-1182, Japan

Abstract

We would like to present our recent work on an enzyme-based biofuel cell, which generates electricity by coupling the anode for oxidation of glucose and the cathode for reduction of oxygen. The peculiar feature of our research is the use of diaphorase / dehydrogenase bi-enzyme system combined with the originally synthesized vitamin K3-based polymer as an electron mediator. MEMS techniques have miniaturized the cells as to be a microfluidic device.

Keywords: Biofuel Cell, Glucose Dehydrogenase, Diaphorase, Vitamin K3

1 Introduction

Fuel cells are the most promising power devices in respect to significant environmental benefits and high electrical efficiency, while most of commercial fuel cell consists of expensive materials such as noble metal catalysts and requires operating temperature over 70 °C [1]. For the power source of implanted medical devices and microrobots, the development of a cheap and safe fuel cell, which operate at physiological condition, have been expected. From this viewpoint, biofuel cells utilizing enzymes as electro-catalyst have been extensively investigated in recent years. Glucose is one of the most attractive fuel owing to its abundance and medical importance. A variety of enzyme / mediator systems have been currently studied [2-5]. For example, Heller *et al.* used glucose oxidase and Os-complex-linked polymer as mediator, and achieved excellent performance (a power density of 350 μW cm^{-2} at a 0.88 V cell potential) under physiological conditions [2, 3], while Os is a handful, most hazardous element.

We have studied the diaphorase (Dp) / dehydrogenase bi-enzyme system as the anode for glucose oxidation, as illustrated in Figure 1. Dp is a flavine-enzyme which converts NADH to NAD$^+$, coenzyme of a variety of dehydrogenase such as the glucose dehydrogenase (GDH). The electron transfer between the electrode an d Dp should be mediated by inexpensive and safe mediators for medical application, and quinine derivatives would meet these demands. Kano and Ikeda revealed that the reaction rate constant between diaphorase (Dp) and mediator is determined by the formal potential of the mediators, and that 3-methyl-1, 4-naphtoquinone (vitamin K3, VK3) is the most promising mediators to ensure the diffusion-limited maximum rate constant [6].
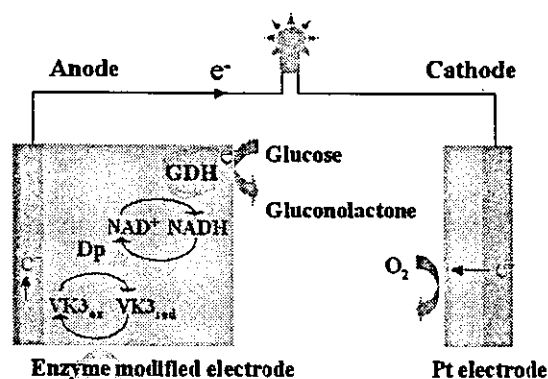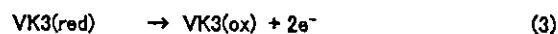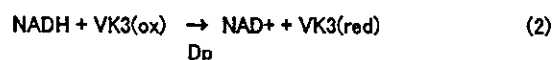

Figure 1. Schematic illustration showing the construction of Dp / GDH biofuel cell and the principle for generating electricity from biofuel (glucose in this case).

The elementary reactions are represented by eqs. (1)-(3).

$$\text{D-glucose} + \text{NAD}^+ \xrightarrow{\text{GDH}} \text{D-gluconolactone} + \text{H}^+ + \text{NADH} \quad (1)$$

$$\text{NADH} + \text{VK3(ox)} \xrightarrow{\text{Dp}} \text{NAD+} + \text{VK3(red)} \quad (2)$$

$$\text{VK3(red)} \rightarrow \text{VK3(ox)} + 2\text{e}^- \quad (3)$$

We will present herein the recent results on the anode performance of the Dp / GDH electrode combined with a VK3-pedanted polymers. The contents are as below;

1) Synthesis of a polymer of VK3 and its co-immobilization with Dp and GDH onto the anode surface

2) Characterization of an oxygen-selective cathode prepared by utilizing the gas-permeable property of PDMS thin film

3) Construction of the microfluidic biofuel cell by coupling the above functionalized electrodes

It should be noted however that the VK3 is known to be O_2-sensitive, which is a drawback for the use in fuel cell system. While the work is still preliminary, we found that the covering the anode electrode with Gox film shows the effect to eliminate dissolving oxygen from the anode. Such the layered structure containing the Gox top layer would be suit for the enzyme electrode with immobilized quinine mediators. These techniques enabled our biofuel cell to be a separator-free system.

2 Experimental

2.1 Chemicals and Materials

Polyallylamine-linked vitamin K3 (PAA-VK3) was newly synthesized by Daiichi Pure Chemicals Co., Ltd. Poly (ethylene-glycol) diglycidyl ether (PEGDGE; average molecular weight is 526) was purchased from Aldrich. Diaphorase (Dp) (from *Bacillus stearothermophilus*, [EC 1.6.99.-], 1090 U/mg) was from Unitika. Glucose dehydrogenase (GDH) (from *bacillus sp.*, [EC 1.1.1.47], 68 U/mg) and Glucose oxidase type-2 (GOD) (from *Aspergillus niger*, [EC 1.1.3.4], 47 U/mg) were from SIGMA. D-(+)-Glucose, potassium nitrate and sodium dihydrogen-phosphate were from Wako. NADH·Na_2 was from Calzyme. These chemicals were used as received. 10 mM phosphate containing 100 mM KNO_3 (PBS) was used as a buffer solution.
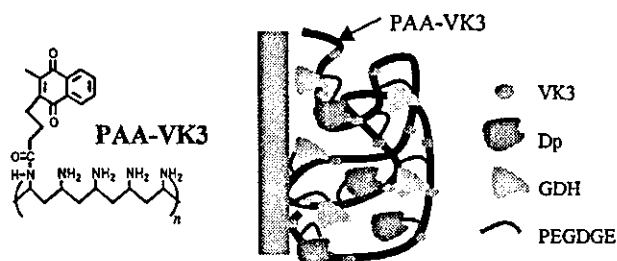

Figure 2. The molecular structure of PAA-VK3, and an illustrated structure of the composite film of Dp, GDH and PAA-VK3 cross-linked by PEGDGE.

2.2 Preparation of Electrodes and Microfluidic Cells

The anode is prepared by dropping PAA-VK3, PEGDGE, Dp and GDH mixture onto the electrode and dried in a desiccator at room temperature for typically 30 min. The epoxide groups of PEGDGE react with amino-groups of the polymer and enzymes and crosslink these elements to form hydrogel film (Figure 2). Anode evaluation was conducted using GC-disk electrode (diameter 3 mm) in a three-electrode system (Hokuto Denko HSV-100 electrochemical analyzer). We used Ag/AgCl (sat. KCl) as a reference electrode and platinum wire as a counter electrode. All measurements were carried out on room temperature (ca. 20 °C).

We used photolithography-based microfabrication techniques to prepare electrode substrates. The microfluidic cell consists of the channel (2 x 28 mm) made of silicon film (0.05 mm in thickness) sandwiched by Au (anode) and Pt (cathode)-sputtered glass plate having an electrode surface area of 0.56 cm^2. A fuel solutions were flowed through the microchannel, and the cell performance was analyzed by measuring cell voltage with changing an inserted variable resistance (0-3 MΩ), as shown in Figure 3.
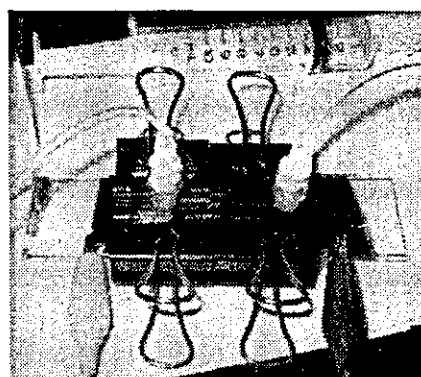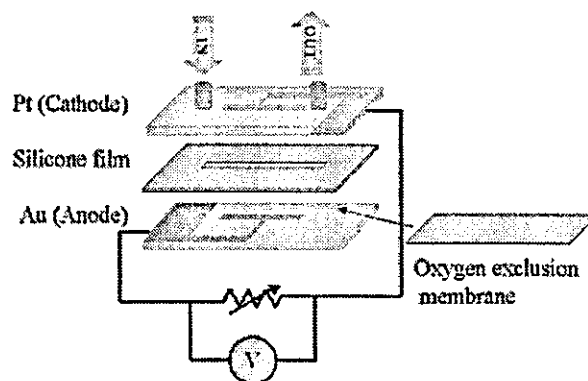

Figure 3. The illustration (upper) and photograph (lower) of the construction of the microfluidic fuel cell to evaluate the performance of enzyme electrode under the steady fuel flow.

3 Results and discussion

3.1 Redox Properties of Anode and Cathode

Figure 4 shows cyclic voltammograms of the PAA-VK3 on GC electrode under nitrogen atmosphere in PBS. Voltammograms showed reversible wave with the half wave potential of -0.25 V vs. Ag/AgCl (at. KCl). The inset shows that oxidation (i_{pa}) and reduction (i_{pc}) peak heights increased almost linearly with the square root of the scan rate of potential ($v^{1/2}$), indicating that the electron can diffuse through the PAA-VK3 hydrogel film by the electron-exchange between the neighboring VK3 units. These features are required for the electron–mediation for the enzymes entrapped within the hydrogel.
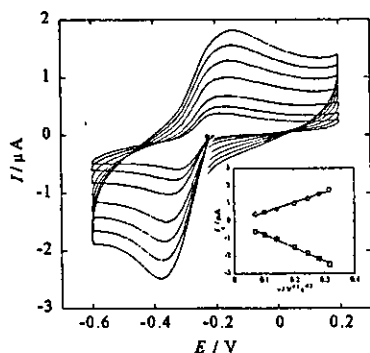

Figure 4. Cyclic voltammograms of PAA-VK3 on GC electrode under nitrogen atmosphere in PBS buffer. Scan rates were 5, 10, 20, 40, 60, 80, 100 mV/s. Inset shows dependence of oxidation and reduction peak heights on the square root of scan rates.

Cathode reaction is the reduction of dissolved oxygen on PDMS-coated Pt electrode, which would be mainly the reduction to hydrogen peroxide. The thin PDMS film on electrode serves as the O_2-selective membrane [7]. The O_2-selective property of cathode would be required upon the use of biofuel containing interfering substance such as ascorbic acid. As showed in Figure 5, peak potential of oxygen reduction was found around +0.25 V vs. Ag/AgCl (sat. KCl). Cell voltage comes from difference of redox potential between mediator and oxygen. Thus the expected cell voltage in roughly 0.5 V for the present system.
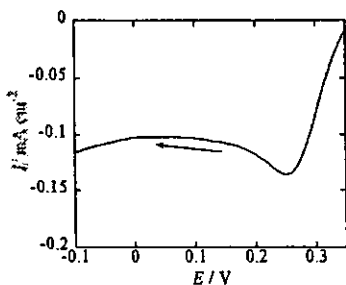

Figure 5. A linear sweep viltammogram for a PDMS-coated Pt plate in air-saturated PBS at 5 mV / s.

3.2 Catalytic Current Generation on Anode

By taking advantage of the enzymatic reactions in the anode membrane, VK3 is expected to be reduced consistently by electron transport shuttle from glucose. We prepared GDH-Dp-PAA-VK3 membrane on GC electrode and measured the cyclic voltammograms of PAA- VK3. In the presence of 0.5 mM NADH, the voltammogram of PAA-VK3 changed to a catalytic wave. Further addition of glucose (final concentration was 10 mM) increased current density of catalytic wave (Figure 6) as the result of chained enzyme reactions.
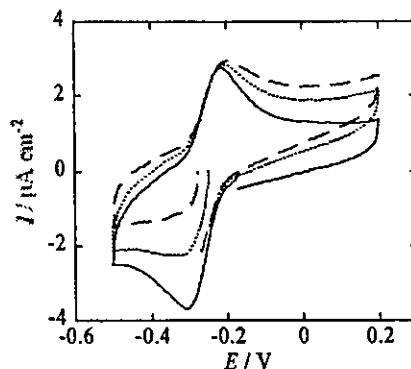

Figure 6. Cyclic voltammograms of the electrode coated with PAA-VK3 - Dp – GDH at 50 mV / s. Buffer only (solid line); 0.5mM NADH (dotted line); 0.5 mM NADH and 10 mM glucose (broken line)

3.3 Evaluation as a Fuel Cell

Using the bi-enzyme-coated anode and the PDMS-coated cathode, we constituted the microfluidic fuel cell shown in Fig. 2. Figure 5 shows dependence of the current density and the power density on the cell voltage. The cell operated at a power density of 0.13 μW cm^{-2} at a 0.15 V cell potential under ambient conditions (air saturated, [glucose] = 5 mM, [NADH] = 1 mM). The observed output potential was significantly lower than the expected value, 0.5 V, due to the O2 sensitivity of VK3. In fact, the voltammetric activity of VK3 disappears in the air-saturated condition, suggesting that oxygen interfere the electrode reaction of VK3.
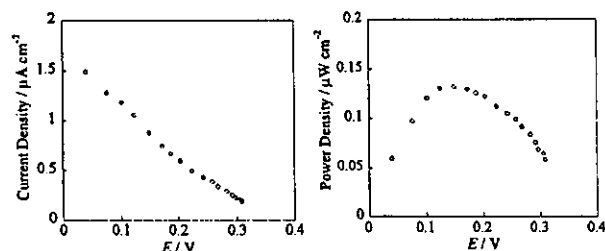

Figure 7. Dependence of the current density (left) and the power density (right) on the voltage of the biofuel cell (pH 7.0, at 25 °C). Fuel is air-saturated PBS containing 5mM glucose and 1 mM NADH.

3.4 Exclusion of Oxygen from Anode

As can be recognized from the results in Fig. 7, it is necessary to exclude oxygen from the vicinity of anode to obtain better performance. For this purpose, we are planning to coat the GDH-Dp bi-enzyme layer with a layer of an oxidase. We covered the anode with glucose oxidase (GOD; negatively charged at pH 7) -immobilized positively charged nylon membrane (Nytran® SuPerCharge), which is expected to consume oxygen with sacrifice of the corresponding amount of glucose.

In order to confirm the effect of GOD layer for eliminating oxygen, we placed it on PAA-VK3–Dp Au electrode and measured its rest potential (Figure 8). At first, we added NADH to PBS, followed by adding glucose. The lowering of the rest potential on the addition of glucose indicates the effective supply of the reduced form of VK3 to the electrode surface. The insertion of this oxidase membrane as a component of the microfluidic cell (see Fig. 1) can be expected to improve the cell performance. Experiments are under progress along this strategy.
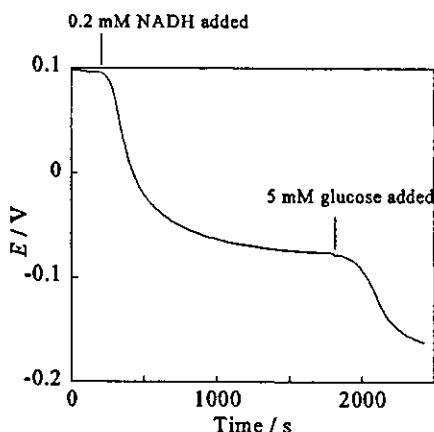

Figure 8. Time courses of the rest potential of PAA-VK3-Dp electrode, which is placed below the GOD membrane. 5 mM glucose followed by the addition of 0.2 mM NADH was added (pH 7, air saturated).

4 Acknowledgement

References

[1] R. M. Ormerod, "Solid Oxide Fuel Cell", *Chem. Soc. Rev.*, **32**, pp. 17-28, 2003.

[2] V. Soukharev, N. Mano, A. Heller, "A four-electron O_2 electroreduction biocatalyst superior to platinum and a biofuel cell operating at 0.88 V", *J. Am. chem. Soc.*, **126**, pp. 8368-8369, 2004.

[3] N. Mano, F. Mao, A. Heller, "Characteristics of a miniature compartment-less glucose-O_2 biofuel cell and its operation in a living plant", *J. Am. chem. Soc.*, **125**, pp. 6588-6594, 2003.

[4] A. Sato, K. Kano, T. Ikeda, "Diaphorase / naphtoquinonederivative-modified electrode as an anode for diffusion-controlled oxidation of NADH in electrochemical cells", *Chem. Lett.*, **32**, pp. 880-881, 2003.

[5] E. Katz, I. Willner, A. B. Kotlyar, "A non-compartmentalized glucose | O_2 biofuel cell by bioengineered electrode surface", *J. Electroanal Chem.*, **479**, pp. 64-68, 1999.

[6] (a) Y. Ogino, K. Takagi, K. Kano, T. Ikeda, "Reactions between diaphorase and quinine compounds in bio-electrocatalytic redox reactions of NADH and NAD^+", *J. Electroanal. Chem.*, **396**, pp. 517-524, 1996.

(b) K. Takagi, K. Kano, T. Ikeda, "Mediated bioelectro- analysis based on NAD-related enzymes with reversible characteristics", *J. Electroanal. Chem.*, **445**, pp. 211-219, 1998.

[7] F. Mizutani, Y. Sato, Y. Hirata, S. Iijima, "Interference-free, amperometric measurement of urea in biological samples using an electrode coated with tri-enzyme/polydimethylsiloxane-bilayer membrane ", *Anal. Chim. Acta*, **441**, pp. 175-181, 2001.

BRIEF COMMUNICATION

Toshihide Mizuno, DVM, PhD
Eisuke Tatsumi, MD, PhD
Tomohiro Nishinaka, MD, PhD · Nobumasa Katagiri, MS
Mitsuo Ohikawa, MD, PhD · Hiroshi Naito, MD
Yukitoshi Shirakawa, MD · Tomonori Tsukiya, PhD
Akihiko Homma, PhD · Yoshinori Takewa, MD, PhD
Hisateru Takano, MD, PhD · Soichiro Kitamura, MD, PhD
Yoshiyuki Taenaka, MD, PhD

Observation of alveolar fibrosis in a goat following venoarterial bypass for up to 5 months using extracorporeal membrane oxygenation

Abstract Prolonged cardiopulmonary bypass such as venoarterial bypass with extracorporeal membrane oxygenation (VA-ECMO) is becoming a potent therapeutic option in treating patients with severe respiratory and circulatory failure. However the chronic effects of this bypass modality have not yet been fully clarified. Recently, we developed an extremely durable thrombo-resistant ECMO system, and were successful with more than 5 months of continuous heparinless VA-ECMO in an animal experiment. This article presents the pathological findings on the lungs of the animal.

A goat underwent VA-ECMO for a scheduled period of 151 days. This animal demonstrated a good general condition during the course of the experiment. On autopsy, however, the lungs of the animal showed severe alveolar fibrosis with topical atelectasis. von Willebrand factor levels on the endothelial cells in the alveolar capillaries were increased compared with those of normal goats. The ultrastructure of these cells showed ischemia-induced endothelial swelling. The pathological findings indicated that the vascular endothelial phenotypes had changed from respiratory type to nutrient type. The results of this study indicated that prolonged VA-ECMO may cause pulmonary alveolar fibrosis as a result of ischemia of the lungs accompanying reduced pulmonary blood flow.

Key words VA-ECMO · Pathology · Alveolar fibrosis · Ischemic change

T. Mizuno (✉) · E. Tatsumi · T. Nishinaka · N. Katagiri ·
M. Ohikawa · H. Naito · Y. Shirakawa · T. Tsukiya · A. Homma ·
Y. Takewa · H. Takano · S. Kitamura · Y. Taenaka
Department of Artificial Organs, National Cardiovascular Center
Research Institute, 5-7-1 Fujishiro-dai, Suita, Osaka 565-8565, Japan
Tel. +81-6-6833-5012; Fax +81-6-6872-8090
e-mail: toshi@ri.ncvc.go.jp

Introduction

Venoarterial bypass extracorporeal membrane oxygenation (VA-ECMO) is becoming a potent therapeutic option in treating patients with severe respiratory and circulatory failure. The use of ECMO has been limited to several days, but recent progress in devices and materials appears to allow longer use of this therapy without an exchange of devices.[1] We have developed an extremely durable antithrombogenic ECMO system that can be used for longer than 1 month without use of systemic anticoagulation.[2] In a series of chronic venoarterial bypass animal experiments, we recently succeeded in performing continuous heparinless ECMO for as long as 5 months; however, the adverse effects of extended VA-ECMO have not been fully clarified. Here we report pathological findings showing severe alveolar fibrosis in the lungs of a goat that underwent VA-ECMO for 5 months.

Materials and methods

A goat weighing 60 kg underwent venoarterial bypass between the right cervical vein and the right atrium using an ECMO system coated by TOYOBO-NCVC coating (Toyobo, Otsu, Shiga, Japan). Systemic anticoagulation was not administrated during the course of the experiment. At the termination of the study (151 days), the goat was enthanased prior to the pathological analysis of the lungs. The samples were fixed immediately in 10% neutral-buffered formalin and embedded in paraffin wax. Thin sections were cut and stained with haematoxylin and eosin, azan, and elastic van Gieson stain and examined immunohistochemically with anti-von Willebrand factor (vWF, Dako, Carpinteria, CA, USA), which was used for characterization of the capillary endothelial cells in the alveolar wall. For electron microscopic examination, trimmed 1-mm cubes of tissue sample were immediately fixed in 1.5% paraformaldehyde and 0.5% glutaraldehyde, followed by

postfixation in 1% osmic acid. The tissue fragments were then embedded in Epon resin. Ultrathin sections were cut with an ultratome (Ultracuts, Leica, Austria), double-stained with uranyl acetate and Sato's basic lead citrate, and examined in a transmission electron microscope (CM120; Philips, Eindhoven, Netherlands).

Results

The animal was maintained in a good condition during this study. The range of bypass flow was maintained at 33–41 ml/min/kg, approximately 30%–40% lower than pulmonary blood flow in a normal adult goat.[3] The PaO_2 and $PaCO_2$ of arterial blood were controlled within the physiologically

acceptable range. We found no characteristic changes such as infarction, thrombosis, or hemorrhaging of the lungs or other internal organs under gross examination during the autopsy, but with microscopy, we observed scattered topical atelectasis in the lungs, and the respiratory bronchioles around these foci was enlarged. The interalveolar tissues of the alveolar walls were thickened at the atelectatic foci in the lung (Fig. 1). The walls showed a marked increase in the interstitial components, which mainly consisted of collagen fibers (Fig. 2); moreover, the elastic fibers were lost.

The capillary endothelial cells showed swelling in the interstitial tissues, and many more endothelial cells showing positive reactions against anti-vWF antibody appeared in the alveolar capillaries compared with those of a normal goat (Fig. 3).

Ultrastructurally, the number of collagen filaments increased in the interstitial tissue of the alveolar wall. Capillary endothelial cells showed swelling, dilated endoplasmic reticulum, mitochondria developing in the enlarged cytoplasm, and a thickened basement membrane .

Discussion and conclusion

In this study, the goat remained in a good condition throughout the 151 days of VA bypass treatment with an ECMO system. However, the lungs of this goat showed severe alveolar fibrosis and topical atelectasis.

The characteristic findings of these lesions were the diffuse proliferation of collagen fibers in the alveolar septum, an increase in the number of anti-vWF-positive capillary endothelial cells, and the nuclear swelling of capillary endothelial cells. These alterations indicate ischemic change of the endothelial cells[4] and phenotypic changes in capillary
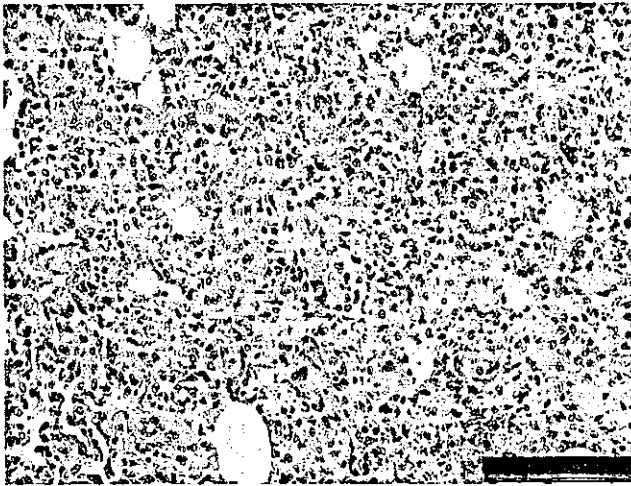

Fig. 1. The lungs showed scattered topical atelectasis and the respiratory bronchiole around these foci were enlarged. Hematoxylin and eosin stain, bar 100 μm

Fig. 2. A Normal structure of the alveolar walls. B Increased collagen fibers in interalveolar tissue. Azan stain, bar 50 μm
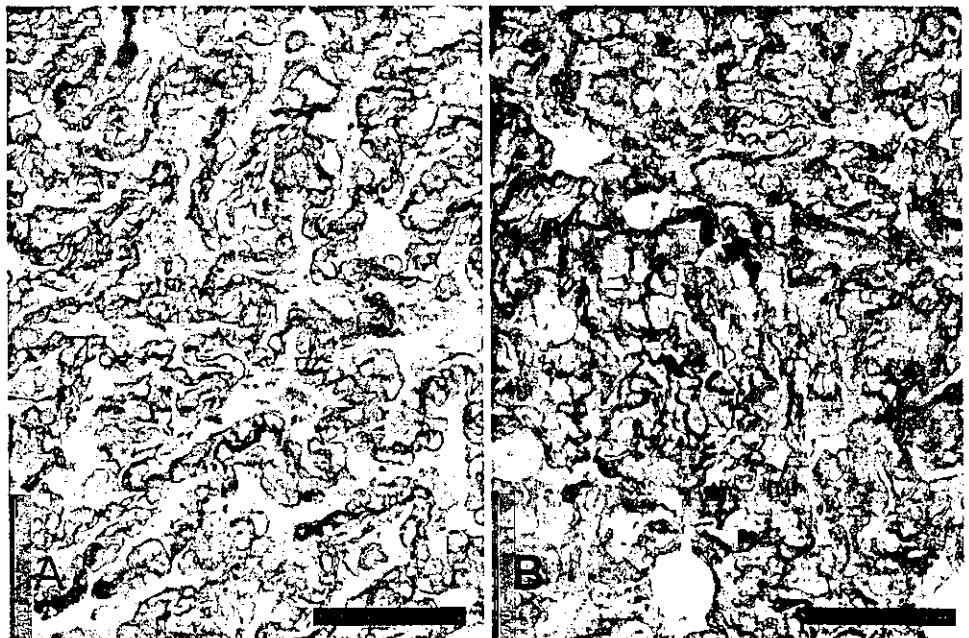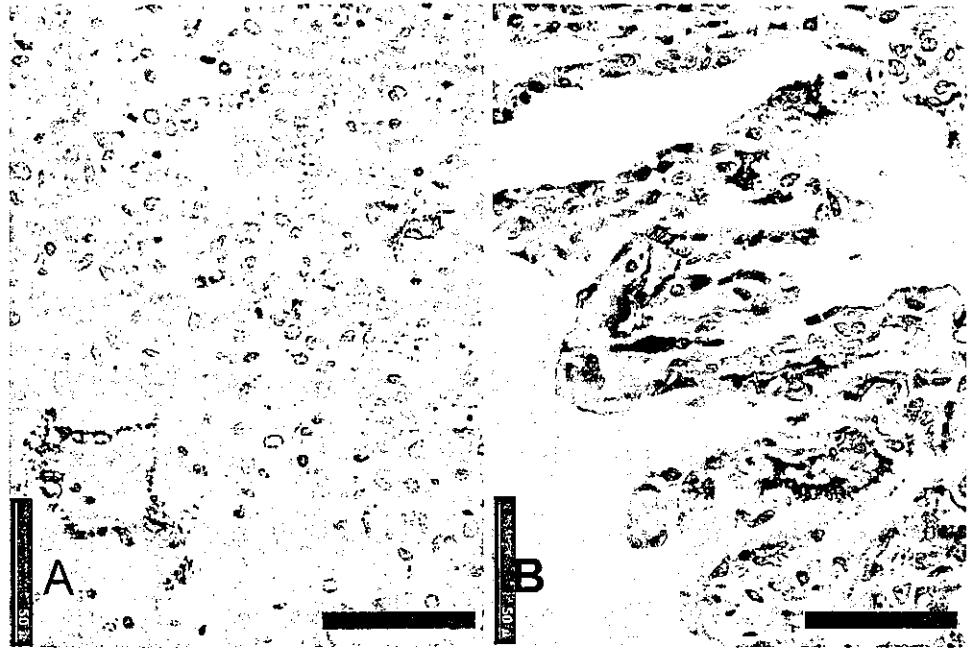
Fig. 3. A Lung tissue treated with anti-von Willbrend factor (VWF) antibody. Normal distribution of vWF on the endothelial cells in the lungs. **B** The lung that underwent 151 days of venoarterial bypass with extracorporeal membrane oxygenation showed a positive reaction against anti-vWF antibody in the alveolar capillaries. *Bar* 50 μm

endothelial cells from the respiratory type to the nutrient type. The phenotypic alterations were similar to the process occurring in interstitial fibrogenesis in tumor cell metastasis and, as defined by the present immunohistochemical study, proceeded in a stepwise manner under microenvironmental influence.[5] These results demonstrated that the pathogenesis of this alveolar fibrosis related to the chronic influence of prolonged reduction of pulmonary blood flow caused by undergoing VA-ECMO. This adverse effect on the lungs relating to prolonged low-flow circulation is a very important factor in the recovery from respiratory failure using VA-ECMO therapy.

References

1. Cornish JD, Wight NE. Complications of neonatal extracorporeal membrane oxygenation. J Pediatr 1990;116:1005

2. Nishinaka T, Tatsumi E, Taenaka Y, Katagiri N, Ohnishi H, Shioya K, Fukuda T, Oshikawa M, Sato K, Tsukiya T, Homma A, Takewa Y, Takano H, Sato M, Kashiwabara S, Tanaka H, Sakai K, Matsuda T. At least thirty-four days of continuous animal perfusion by a newly developed extracorporeal membrane oxygenation system without systemic anticoagulants. Artif Organs 2002;26:548–551

3. Takewa Y, Tatsumi E, Taenaka Y, Eya K, Nakatani T, Nishimura T, Sohn YS, Masuzawa T, Wakisaka Y, Nakamura M, Endo S, Takano H, Kitamura S. Hemodynamic and hormonal condition in stepwise reduction of pulmonary blood flow during venoarterial bypass in an awake goat. ASAIO J 1997;43:M494–M499

4. Mazzoni MC, Borgstrom P, Warnke KC, Skalak TC, Intaglietta M, Arfors KE. Mechanisms and implications of capillary endothelial swelling and luminal narrowing in low-flow ischemias. Int J Microcirc Clin Exp 1995;15:265–270

5. Jin E, Ghazizadeh M, Fujiwara M, Nagashima M, Shimizu H, Ohaki Y, Arai S, Gomibuchi M, Takemura T, Kawanami O. Angiogenesis and phenotypic alteration of alveolar capillary endothelium in areas of neoplastic cell spread in primary lung adenocarcinoma. Pathol Int 2001;51:691–700

CONSTRUCTION OF LIVER MODEL WITH GENETICALLY ENGINEERED HUMAN HEPG2 CELLS

Takeshi Omasa [1], and Shin Enosawa [2]*
1 *Dept. of Biotechnology; Graduate School of Engineering; Osaka University; 2-1 Yamadaoka; Suita, Osaka 565-0871; Japan*
2 *National Research Institute for Child Health and Development; Setagaya-ku, Tokyo; 154-8509; Japan*
Corresponding author. E-mail: senosawa@nch.go.jp

ABSTRACT: Bioartificial liver (BAL) support systems are currently expected to be novel therapeutic devices for the end stage of hepatic failure. Treatment with BAL systems will improve recipient conditions as a bridge to successful transplantation and will support the critical stage of the post-operational period. We developed a BAL system containing the human hepatoblastoma cell line HepG2 with the addition of an ammonia removal function by transfecting a glutamine synthetase (GS) gene. After transfection of a hamster GS gene into HepG2, the resulting GS-HepG2 cells showed 15% ammonia removal activity of porcine hepatocytes, while unmodified HepG2 cells had no such activity. The established GS-HepG2 cells were grown in a circulatory flow bioreactor and used when the cell numbers reached $3.5 - 4.1 \times 10^9$. We used pigs with ischemic liver failure to estimate the efficiency of the BAL system. The BAL treatment was started 3 hrs after the completion of total liver ischemia. The survival time of the animals treated with GS-HepG2 BAL was significantly longer than that of the cell-free control group (14.5 hrs vs. 8.5 hrs) and the group treated with BAL consisting of unmodified HepG2 (9.6 hrs). The BAL groups containing the GS-HepG2 cells had significantly fewer incidents of increased brain pressure and abnormalities of coagulation indices during the plasma exchange treatment.

Since the efficacy of BAL is regulated not only by cell capability but also by module specification, we estimated the xenobiotic clearance of our BAL system by using newly developed GS-3A4-HepG2, which was transduced with the CYP3A4 gene. The 3A4 activity reached 430 pmol/min/mg-protein in GS-3A4-HepG2, which was approximately 1.7 times that of human hepatocytes in primary culture. The lidocaine clearance of the entire BAL system was calculated to be 8.0 ml/min, while that of another BAL system with isolated porcine hepatocytes was reported to be 46 ml/min [1]. Further improvements will require control of the rate of blood circulation and the use of high-density cultures.

K.Yagasaki et al. (eds), Animal Cell Technology: Basic & Applied Aspects, Volume 13,25-29

©2004 Kluwer Academic Publishers. Printed in the Netherlands.

1. Introduction

Recently, a hybrid bioartificial liver (BAL) support system composed of artificial materials and living cells, was developed as a stopgap measure for use in patients with hepatic failure. Heretofore, primary xenogeneic hepatocytes, for instance, porcine hepatocytes, have been the major cell type used to support human liver functions in BAL systems [2]. Recently, however, the possibility of unknown animal-origin retrovirus infection from these xenobiotic hepatocytes has become a growing concern. Hepatoma-derived cell lines are suitable for long-term use because of their near-infinite capacity for proliferation and no risk of xenozoonosi [3]. These cell lines frequently lose some liver cell functions, particularly the ability to metabolize ammonia [4]. Ammonia is considered one of the major causes of hepatic encephalopathy, which is among the most serious pathophysiological features of fulminant hepatic failure. Hemodialysis and/or plasmapheresis have been used for ammonia removal but neither can accomplish selective removal of ammonia. In this study, we constructed ammonia- and drug-removing hepatoma-derived HepG2 cell lines by recombination and gene amplification of the GS and CYP3A4 genes for long-term use in a BAL system.

2. Materials and Methods

2.1 CELL LINE, MEDIUM, AND CONSTRUCTION OF RECOMBINANT CELL LINES

The host cell line employed in the experiments was HepG2 (RCB0459). The expression vector, pBK-CMV-GS, was constructed by insertion of the GS gene into the pBK-CMV (Stratagene 212209) vector. The HepG2 cells were transformed with the pBK-CMV-GS vector by lipofection. The recombinant cells were selected under several different concentrations of the GS inhibitor, methionine sulfoximine (MSX). For the drug-metabolizing cell line, the expression vector, pBudCE-GS-CYP3A4, was constructed by insertion of the GS and CYP3A4 genes (based on pLNCX-CYP3A4, which was kindly donated by Dr. Grone) into the pBudCE (Invitrogen V532-20) vector. Evaluation of the ammonia-metabolizing activity was performed in a T-flask culture (medium volume: 90 ml). The cell concentration was measured by photomicrography. The kinetic parameters were analyzed as described previously [5]. Evaluation of the specific drug metabolizing activity of the CYP3A4 was based on testosterone 6β-hydroxylation.

2.2 HYBRID BIOARTIFICIAL LIVER SUPPORT SYSTEM

Construction of the hybrid bioartificial liver (BAL) support system was based on a high-density cell culture system with a system working volume of 1.0 ℓ. A roll of 5 cm × 3 m glass-fiber cloth was placed in the reactor vessel. The pH and concentration of dissolved oxygen were monitored and controlled (Fig. 1).
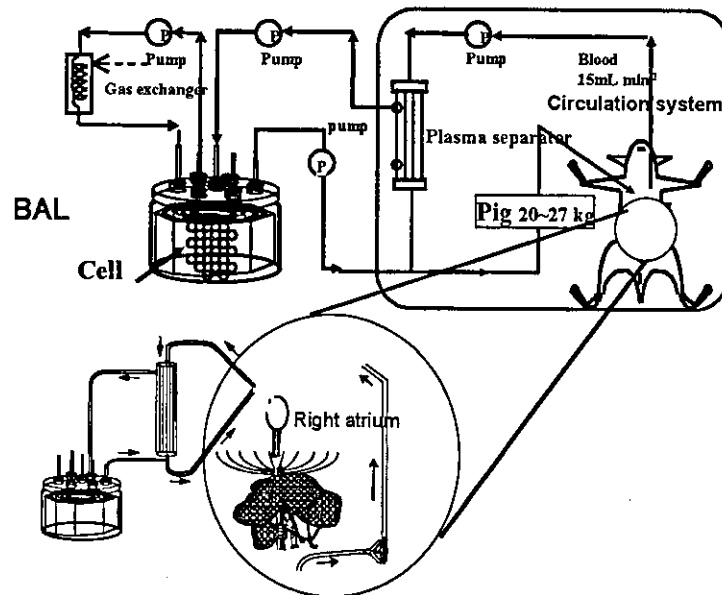
Figure 1. Bioartificial liver support system for ischemic hepatic failure in pig [6-8].

3. Results and Discussion

3.1 CONSTRUCTION AND EVALUATION OF AMMONIA METABOLIZING CELL LINE

In the liver, selective removal of ammonia is primarily achieved by the urea cycle. The GS reaction is used as a secondary metabolic pathway for the removal of ammonia in the liver. GS can also be amplified in CHO (Chinese hamster ovary) cells under selection by the GS inhibitor, methionine sulfoximine (MSX).

Hepatoma-derived HepG2 cells were transformed with the pBK-CMV-GS vector containing the GS gene with the CMV promoter. The amplification efficiency of the GS gene was strongly influenced by an increase in MSX concentration. In this study, based on the dhfr-MTX gene amplification techniques in our previous work, the MSX concentration was gradually increased during selection. Since no studies have so far reported GS gene amplification in the HepG2 cell line, the same method as that used for the previous CHO cell line, using increasing concentrations of MSX, was applied to the HepG2 cell line. With increased MSX concentration in the medium, the GS activity increased slightly, to 2.5 times that of the host HepG2 cell line (13×10^{-6} units cell^{-1}). Among the MSX-tolerant cell lines, we selected the 200-μM MSX-tolerant cell line based not only on GS activity but also on growth rate, because the growth rates of

highly MSX-tolerant cell lines are too low for effective use in a BAL system.

The rate of ammonia consumption in the constructed HepG2 cell line was about 15% of the rate in primary hepatocytes. By using a tandem vector, the GS gene amplification system can be used to amplify other useful genes in addition to the GS gene. Gene amplification enables the construction of HepG2 cell lines with not only ammonia-metabolizing activity but also other liver functions.

3.2 BIOARTIFICIAL LIVER SUPPORT SYSTEM FOR ISCHEMIC HEPATIC FAILURE [6-8]

We constructed and evaluated a BAL system that employed a recombinant cell line. The established GS-HepG2 cells were grown in a circulatory flow bioreactor and used when the cell numbers reached $3.5 - 4.1 \times 10^9$. We estimated the efficiency of the BAL using pigs with ischemic liver failure. BAL treatment was started 3 hrs after the completion of total liver ischemia. The survival time of the animals treated with the GS-HepG2 BAL system was significantly longer than that of the cell-free control (14.5 hrs vs. 8.5 hrs) and that of a group treated with a BAL system consisting of unmodified HepG2 (9.6 hrs). The BAL groups containing the GS-HepG2 cells had significantly fewer incidents of increased brain pressure and abnormalities of coagulation indices during the plasma exchange treatment.

3.3 EVALUATION OF BIOARTIFICIAL LIVER SUPPORT SYSTEM BASED ON THE XENOBIOTICS CLEARANCE

To further improve the constructed cell line, we attempted to increase the drug metabolizing activity by adding rifampicin. With an increase of the rifampicin concentration in the medium, the testosterone 6β-hydroxylation activity of GS-HepG2 increased. However, the induced activity was one thirtieth of that of the primary hepatocytes. For the construction of other functional cell lines in hybrid bioartificial liver support systems, HepG2 cells were transformed by the pBudCE-GS-CYP3A4 vector, which contains the GS and CYP3A4 genes, the GS-3A4-HepG2 cell line was constructed. The testosterone 6β-hydroxylation activity reached 430 pmol/min/mg-protein in GS-3A4-HepG2, which is approximately 1.7 times that of human hepatocytes in primary culture. To evaluate the overall drug-metabolizing capability of a BAL system using the GS-3A4-HepG2 cell line, we calculated the xenobiotic clearance based on Hoener's method using equations (1) and (2), below [9].

$$CL_{INT} = \frac{V_{MAX}}{K_m + \alpha C} \qquad (1)$$

$$CL_{BAL} = \frac{Q\alpha CL_{INT}}{Q + \alpha CL_{INT}} \qquad (2)$$

The lidocaine clearance of the entire BAL system (CL_{BAL}) was calculated to be 8.0 ml/min, while another BAL system with isolated porcine hepatocytes was 46 ml/min [1]. Further improvement will require control of the rate of blood circulation and the use of high-density cultures.

5. Nomenclature (values of present report are shown in parentheses)

CL_{INT}: BAL intrinsic clearance

CL_{BAL}: BAL clearance

V_{MAX}: lidocaine metabolizing activity
= total number of cells x specific activity (4×10^9 cells $\times$ 5.1 nmol/min/mg-protein)

K_m: Michaelis-Menten parameter (65 µM)

C: Drug concentration in the blood (83 µM)

α: Fraction of drug unbound in blood (= 0.3 in lidocaine)

Q: Blood flow rate (= 15 mL/min in our BAL system)

6. References

[1]Iwata, H., Sajiki, T., Maeda, H., Park, Y.G., Zhu, B., Satoh, S., Uesugi, T., Ikai, L, Yamaoka, Y., and Ikada Y. (1999). *In Vitro* evaluation of metabolic functions of a bioartificial liver. *ASAIO Journal* 45, 299-306.

[2]Rozga, J. and Demetriou, A. A. (1995) Artificial liver. Evolution and future perspectives *ASAIO Journal*, 41, 831-837.

[3]Sussuman, N.L. and Kelly, J.H. (1993) Artificial liver: a forthcoming attraction *Hepatology*, 17, 1163-1164.

[4]Enosawa, S., Suzuki, S., Kakefuda, T., and Amemiya, H (1996) Examination of 7-ethoxycoumarin deethylation and ammonia removal activities in 31 hepatocyte cell lines *Cell transplant.* 5, S39-S40.

[5] Omasa, T., Higashiyama, K., Shioya, S., and Suga, K. (1992) Effect of lactate concentration on hybridoma culture in lactate-controlled fed-batch operation *Biotechnol. Bioeng.* 39,556-564.

[6]Miyashita, T., Enosawa, S., Suzuki, S., Tamura, A., Tanaka, H., Amemiya, H., Matsumura, T., Omasa, T., Suga, K., Aoki, T., and Koyanagi, Y. (2000) Development of a bioartificial liver with glutamine synthetase-transduced recombinant human hepatoblastoma cell line, HepG2 *Transplant Proc.*, 32, 2355-2358.

[7]Enosawa, S., Mukaiyama, T., Miyashita, T., Li, X.,-K., Suzuki, S., Amemiya, H., Matsumura, T., Omasa, T., and Suga, K. (2001) Application of circulatory flow bioreactor for long-term and large-scale culture of glutamine synthetase transduced CHO cells and its ammonia removal activity with an aim of development for a bioartificial liver assist system, *Journal of Artificial Organ* 4, 61-66.

[8]Enosawa, S., Miyashita, T., Fujita, Y., Suzuki, S., Amemiya, H., Omasa, T., Hiramatsu, S., Suga, K., and Matsumura, T. (2001) In vitro estimation of bioartificial liver with recombinant HepG2 cells using pigs with ischemic liver failure, *Cell transplant.* 10, 429-433

[9]Hoener, B.A. (1994) Predicting the hepatic clearance of xenobiotics in humans from *in vitro* data. *Biopharmaceutics drug disposition* 15, 295-304.

4. Acknowledgments

Transplantation of Nonvascularized Kidney Tissue Fragments Into the Rat Liver With the Aim of Preserving Renal Function

Shin Enosawa,* Nanae Takahashi,* Hiroshi Amemiya,† and Yoshihiro Motomiya†

*Department of Innovative Surgery, National Research Institute for Child Health and Development, Tokyo, Japan
†Suiyukai Clinic, Nara, Japan

For research in regenerative medicine, not only the study of cellular pluripotency but also knowledge of the reorganization of tissue structure is crucial. However, the latter will probably be more difficult to acquire. When small fragments of kidney (approx. 1 × 1 mm) were implanted in the liver of syngeneic LEW rats, the tissue survived at least 2 weeks with retention of normal structure including glomeruli and tubules. In contrast, no kidney structure survived when transplanted to subcutaneous sites, omentum, or spleen. Molecules involved in renal tubular function, such as megalin and glut2 transporter protein, were detectable in the implanted tissue by immunohistochemistry, suggesting that the cells were biologically active. Survival of cortex, medulla, and calyx tissues was then compared. All three components were still detectable 8 weeks after transplantation but cortex and medulla were replaced by granuloma at 6 months. Only calyx tissue survived for up to 12 months after transplantation. There was no marked difference in tissue survival, either when the recipient liver was partially resected or when infantile donor kidney was implanted instead of adult kidney. The present method opens new avenues in the development of regenerative medicine (i.e., tissue transplantation) as an intermediate modus between organ transplantation and cell transplantation.

Key words: Tissue transplantation; Kidney; Rat; Megalin

INTRODUCTION

End stage of renal failure is no longer a life-threatening disease for most patients now that hemodialysis and peritoneal dialysis are widely available (1). However, hemodialysis as presently practiced substitutes for only a limited range of kidney functions (i.e., management of water and ion balance and removal of low molecular weight metabolic end products, such as urea, creatinine, etc.). Other renal functions, such as erythropoietin production and activation of vitamin D, have to be substituted exogenously. Progress in treatment has led to increasing numbers of long-term survivors among patients without kidney function, and this makes another complication, dialysis-related amyloidosis, more urgent (6,17). The latter syndrome is characterized by the accumulation of amyloid substances around joints and peritendon areas accompanied by dyskinesia and severe pain, resulting in marked reduction of patients' quality of life. Because the amyloid precursor, β_2-microglobulin produced mainly by lymphocytes, is catabolized by the renal proximal tubular cells, kidney transplantation is the most effective treatment, although high-performance

membrane dialysis and acetyl amine affinity column (Lixell, Kaneka, Osaka, Japan) have been introduced to prevent the accumulation of β_2-microglobulin in the blood of hemodialysis patients (7).

While kidney transplantation is the most effective treatment for renal failure, donor shortage is a worldwide problem. Thus, it is hoped that regenerative medicine may eventually replace organ transplantation. However, despite strenuous efforts of researchers thus far, organ reconstruction at therapeutically useful levels has not been accomplished. One factor that is thought to impede the survival and function of transplanted cells is that the cells establish themselves poorly at the graft site and are eliminated in a nonimmunological manner. Experimentally, hepatocyte transplantation succeeds only if the host liver is damaged beforehand by irradiation (8), hepatotoxins (14,16), induction of apoptosis (13), or introduction of hepatotoxic transgenes (2,3). Needless to say, these protocols are not practicable in the clinical situation.

Tissue transplantation is an attractive alternative to compensate for the disadvantages of organ or cell transplantation. To this end, we conducted kidney tissue

transplantation experiments and found that the tissue survived long term and retained histological characteristics of kidney.

MATERIALS AND METHODS

Animals and Surgical Procedures

Inbred LEW rats (specific pathogen free, SEAC Yoshitomi, Fukuoka, Japan) were used throughout the experiments. All experimental procedures were designed according to our institutional animal ethics guidelines based on those of the NIH (18). Kidneys were taken from 2-day-old to 14-week-old rats under ether anesthesia and pieces excised approximately 1×1 mm or less in size from cortex, medulla, and calyx (Fig. 1). Recipient liver was cut to make a small pouch by microforceps just beneath the serosa and a fragment of kidney tissue was inserted into the pouch. The open end of the pouch was sutured with 7-0 polypropylene needle-suture (3/8 9.5-mm 7-0, Kyowa Co. Ltd, Chiba, Japan) to stop bleeding and to mark the site of transplantation. No modification of kidney function of recipient rats was performed. In preliminary experiments, kidney fragments were implanted in subcutaneous tissue, spleen, omentum, or remnant liver remaining after partial (70%) resection at the time of implantation. The transplanted tissue was harvested en bloc at 2, 4, or 8 weeks or 6 or 12 months after grafting. Each experiment was performed with three to four rats. The tissue was fixed with 5% neutralized formalin for hematoxylin and eosin staining or quickly frozen in OCT compound (Sakura Finetek, Tokyo, Japan), using liquid nitrogen for immunohistochemistry.

Antibodies

Anti-megalin polyclonal antibodies were obtained by immunizing rabbits with a mixture of two different parts of synthetic peptides (20 and 16 mer; amino acid sequences 4251–4269 and 4289–4303) conjugated with keyhole limpet hemocyanin. The antiserum was purified to IgG by protein G (Mab Trap, Amersham Biosciences, Piscataway, NJ) before use.

Histological Examination

A thin cryocut section of the frozen samples was stained with rabbit polyclonal antibodies specific for megalin or glut2 (sc-9117, Santa Cruz Biotechnology, Santa Cruz, CA) as primary antibodies. Briefly, the slides were air dried and fixed in acetone, then stained with primary antibody diluted to 1/200 in phosphate-buffered saline containing 2% bovine serum and 0.1% sodium azide at 4°C overnight. Thereafter, we incubated the slides with a secondary antibody, horse radish peroxidase-conjugated goat anti-rabbit IgG (sc-2004, Santa Cruz Biotechnology) diluted 1/100 in the above working solution. Color development was done with diaminobenzidine (Dojin Chemicals, Osaka, Japan).

RESULTS

Transplanted renal tissue was found almost intact in the liver 2 weeks after introduction in all recipients (n = 3) (Fig. 2A). Tissue transplanted to other sites, such as subcutaneous tissue, spleen, or omentum, disappeared completely, probably due to nonspecific inflammatory elimination or insufficient supply of nutrients. In contrast, there was no necrotic area in the transplanted tis-
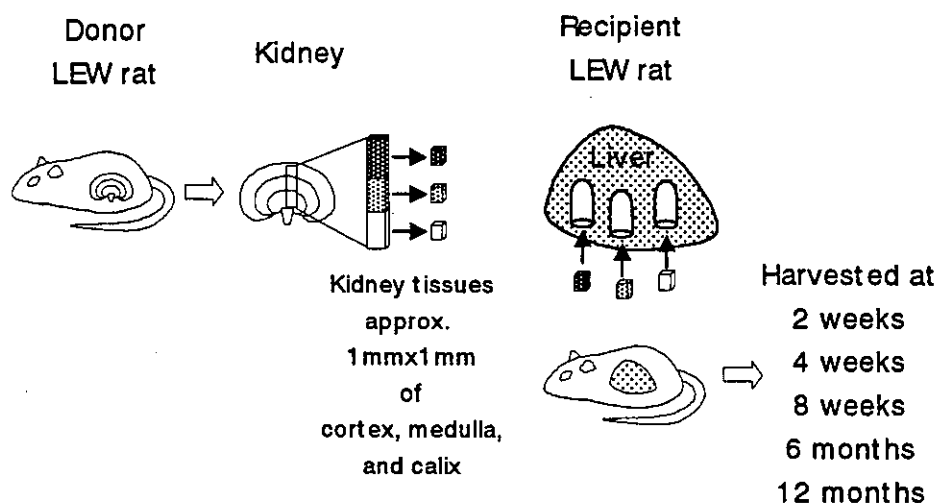

Donor
LEW rat   Kidney

Recipient
LEW rat

Kidney tissues
approx.
1mmx1mm
of
cortex, medulla,
and calix

Harvested at
2 weeks
4 weeks
8 weeks
6 months
12 months

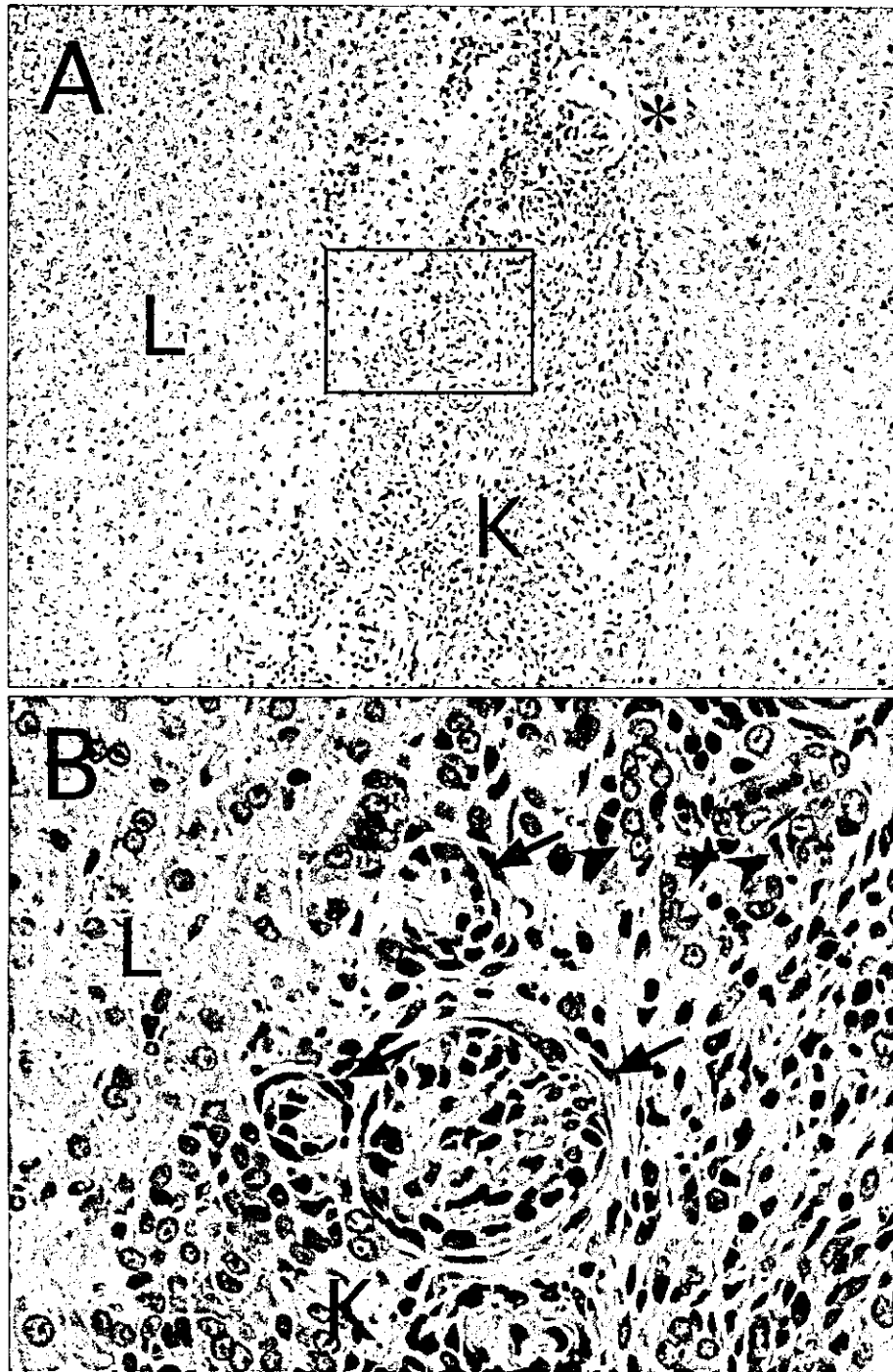Figure 1. Outline of surgical procedures and experimental design.

Figure 2. (A) Histology of transplanted kidney tissue (cortex) at 2 weeks after grafting. L, host liver; K, transplanted kidney. Asterisk indicates a glomerulus secreting serous material. Original magnification: ×40. (B) Magnified view of area indicated in (A). Arrows indicate glomeruli and arrowheads renal tubules. Original magnification: ×200.
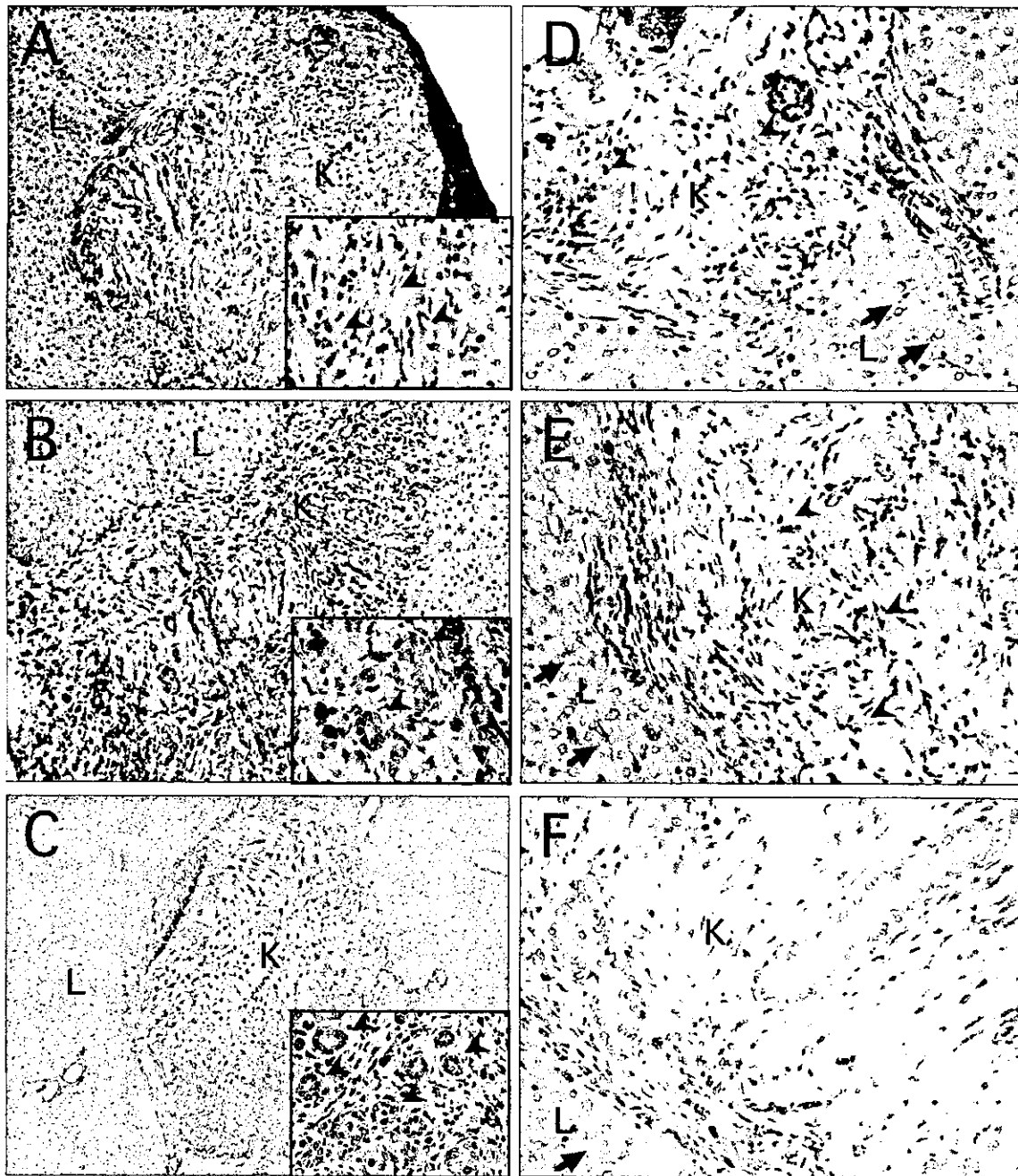
Figure 3. Immunohistochemistry of transplanted kidney tissue for megalin (A, B, C) and glucose transporter 2 (D, E, F). Cortex (A, D), medulla (B, E), and calyx (C, F) were transplanted and harvested 4 weeks later. L, host liver; K, transplanted kidney. Arrowheads indicate positively stained cells. Arrows indicate positively stained glucose transporter 2 on hepatocytes (D, E, F). Original magnification: (A) ×100, (B) ×100, (C) ×40 (insets in A, B, C: ×400), (D–F) ×200.

sue and renal structure was well preserved, including glomeruli and tubules (Fig. 2B). In addition, one glomerus was probably still able to secrete serous material (Fig. 2A, asterisk).

Immunohistochemically, megalin, an endocytosis receptor for macromolecules including β_2-microglobulin

(11), was detectable in tubules especially in the medulla and calyx 4 weeks after transplantation (Fig. 3B, C). The staining intensity was slightly lower in the cortex, due to low expression of the protein or reduced frequency of surviving cells (Fig. 3A). On the other hand, the glucose transporter, glut2, a typical marker of proximal tubule

(4), was positive on the cells in cortex and medulla, but virtually negative in calyx (Fig. 3D-F).

The difference in survival in different renal areas is shown in Figure 4. Cortex, medulla, and calyx components were all still found in the liver 8 weeks after trans-

plantation (Fig. 4A-C). All three components were detectable 8 weeks after grafting (tissue survival rate: 3/3 in Fig. 4A-C). Only calyx was found 6 months (Fig. 4D) and 12 months (Fig. 4E) after grafting (tissue survival rate; 2/3 in Fig. 4D and 2/2 in Fig. 4E). The tubule

Figure 4. Comparison of survival of different areas of the kidney. Cortex (A), medulla (B), and calyx (C) were detectable 8 weeks after grafting (tissue survival rate: 3/3 in A, B, and C). Only calyx was found 6 months (D) and 12 months (E) after grafting (tissue survival rate: 2/3 in case D and 2/2 in case E). The tubule structure was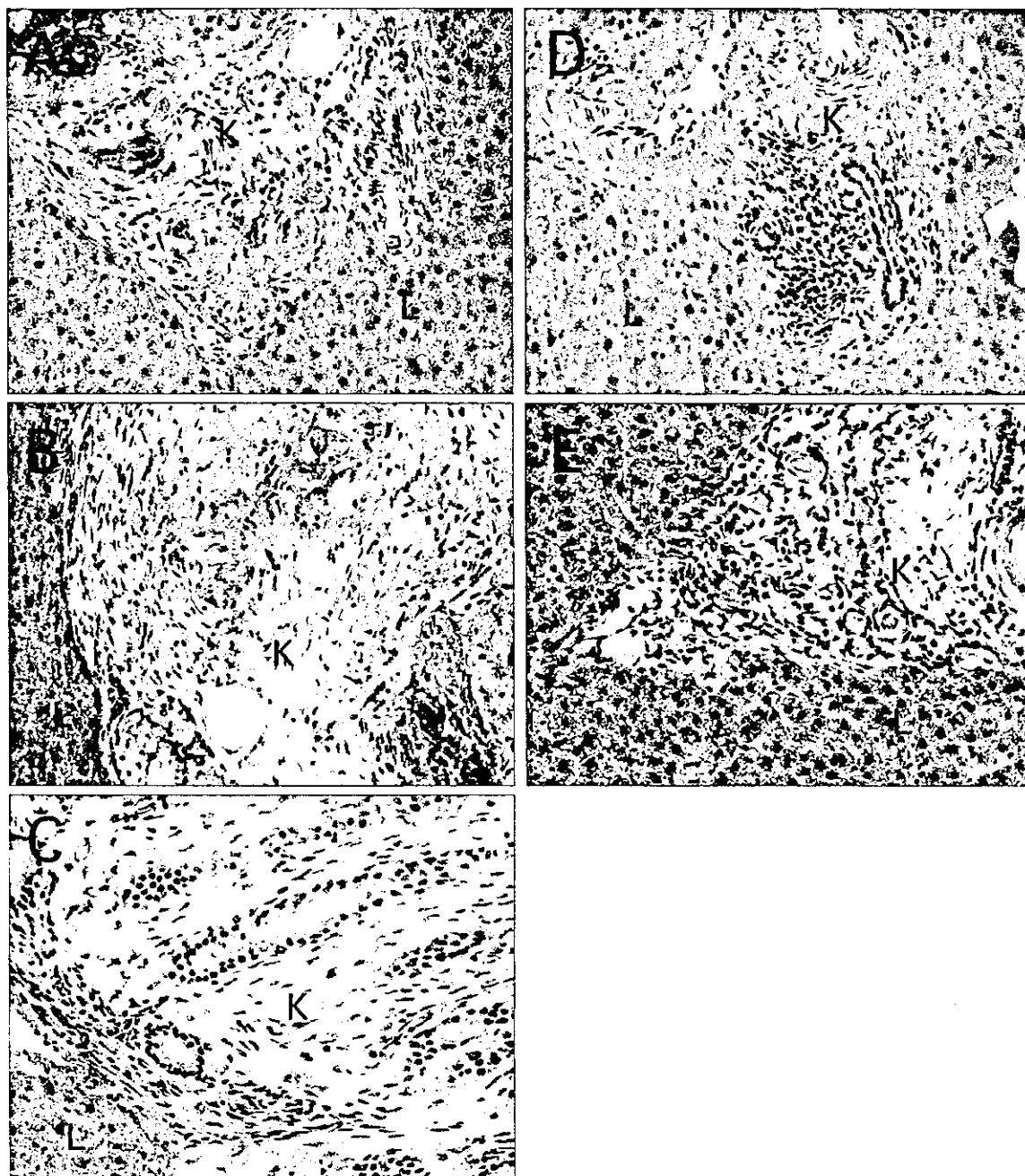 well preserved in calyx at all times. Implantation was performed with three rats in each group. The survival rate is the number of survivors/number of implanted rats. L, host liver; K, transplanted kidney. Original magnification ×200.

structure was well preserved in calyx at all times, whereas cortex and medulla disappeared or were replaced by granuloma. In preliminary experiments, partial (70%) hepatectomy was performed at the time of tissue transplantation, with the expectation that increased levels of hepatocyte growth factor (HGF) might contribute to survival and proliferation of the transplanted tissue, because HGF has been reported to activate growth and recovery of kidney cells (12). However, no detectable effect on tissue survival was observed. In addition, tissue from infantile kidney (2 days after birth) did not show marked prolongation of survival or enlargement of the tissue. The only factor thus far identified as likely to influence the fate of the graft is the size of the transplanted tissue fragment. No tissue larger than 1 × 1 mm in size survived in the liver.

DISCUSSION

In animal experiments, nonvascularized transplantation or transplantation without vascular anastomosis has been tested for several tissues, including thymus in the kidney, trachea and small intestine in subcutaneous tissue, and myocardium in the auricle. Transplantation of isolated islets of Langerhans into the liver or kidney is also a type of nonvascularized tissue transplantation. Clinically, tissue transplantation is performed with cornea, skin, bone, cardiac valve, and islet. However, there are no reports on survival of kidney fragments transplanted into another organ.

Our aim is to support patients with renal failure by preserving certain kidney functions in the liver. The proposed advantage of this approach is the biological removal of β_2-microglobulin by megalin-mediated endocytosis to prevent dialysis-related amyloidosis. In some renal diseases such as diabetic renal dysfunction and IgA nephritis, glomerular damage precedes tubular destruction. When the patient is put on hemodialysis, it is proposed that a portion of kidney tissue should be transplanted to the liver to support renal functions other than glomerular filtration.

In addition to the above-mentioned protocol of autotransplantation, another possible clinical application of kidney tissue transplantation is the use of organs suboptimal for organ transplantation. Hepatocyte transplantation to the Crigler-Najjar syndrome patient mentioned above was performed with liver that was not suitable for organ transplantation (5). The hepatocytes were prepared from a donor liver that was not suitable for organ transplantation and the treatment succeeded in reducing serum bilirubin level. Utilization of suboptimal organs would at least solve the problem of donor shortage. For instance, the use of infantile kidney donors is not encouraged for adult recipients because of their small size and physiological immaturity. Indeed, donor age less

than 1 year is a known risk factor for graft loss (15). These marginal or even less than marginal donors could nonetheless still represent a source of tissue for transplantation of organ fragments and, at the same time, the statement of "gift-of-life wish" by organ donors will be satisfied.

Unlike organ transplantation, in which the whole organ is replaced, tissue or cell transplantation is of low risk even if the graft is rejected, because most patients can survive with their own organs for a while. Therefore, patients are able to wait for reviving or repopulating cells. In this sense, tissue or cell transplantation will be suitable either for the therapy of chronic disease or prophylactic treatment against latent disease, such as dialysis-related amyloidosis. The development of extracorporeal bioartificial kidneys is a current topic in the field of artificial organs, aiming to overcome the limitation of present hemodialysis treatment (9,10). Harmonization of technology developed in the tissue engineering used for assembling of artificial organs and tissue transplantation may contribute to achieving optimal immunoisolation with retention of high-performance biological activities, resulting in an innovation in regenerative medicine.

REFERENCES

1. Becker, B. N.; Stone, W. J. Options for renal replacement therapy: Special considerations. Semin. Nephrol. 17(3): 176–187; 1997.
2. Braun, K. M.; Degen, J. L.; Sandgren, E. P. Hepatocyte transplantation in a model of toxin-induced liver disease: Variable therapeutic effect during replacement of damaged parenchyma by donor cells. Nat. Med. 6(3):320–326; 2000.
3. Dandri, M.; Burda, M. R.; Torok, E.; Pollok, J. M.; Iwanska, A.; Sommer, G.; Rogiers, X.; Rogler, C. E.; Gupta, S.; Will, H.; Greten, H.; Petersen, J. Repopulation of mouse liver with human hepatocytes and in vivo infection with hepatitis B virus. Hepatology 33(4):981–988; 2001.
4. Dominguez, J. H.; Camp, K.; Maianu, L.; Garvey, W. T. Glucose transporters of rat proximal tubule: Differential expression and subcellular distribution. Am. J. Physiol. 262(5 Pt. 2):F807–812; 1992.
5. Fox, I. J.; Chowdhury, J. R.; Kaufman, S. S.; Goertzen, T. C.; Chowdhury, N. R.; Warkentin, P. I.; Dorko, K.; Sauter, B. V.; Strom, S. C. Treatment of the Crigler-Najjar syndrome type I with hepatocyte transplantation. N. Engl. J. Med. 338(20):1422–1426; 1998.
6. Freemont, A. J. The pathology of dialysis. Semin. Dial. 15(4):227–231; 2002.
7. Furuyoshi, S.; Nakatani, M.; Taman, J.; Kutsuki, H.; Takata, S.; Tani, N. New adsorption column (Lixelle) to eliminate beta2-microglobulin for direct hemoperfusion. Ther. Apher. 2(1):13–17; 1998.
8. Guha, C.; Parashar, B.; Deb, N. J.; Garg, M.; Gorla, G. R.; Singh, A.; Roy-Chowdhury, N.; Vikram, B.; Roy-Chowdhury, J. Normal hepatocytes correct serum bilirubin after repopulation of Gunn rat liver subjected to irradiation/partial resection. Hepatology 36(2):354–362; 2002.

9. Humes, H. D.; Buffington, D. A.; MacKay, S. M.; Funke, A. J.; Weitzel, W. F. Replacement of renal function in uremic animals with a tissue-engineered kidney. Nat. Biotechnol. 17(5):451–455; 1999.

10. Kanai, N.; Fujita, Y.; Kakuta, T.; Saito, A. The effects of various extracellular matrices on renal cell attachment to polymer surfaces during the development of bioartificial renal tubules. Artif. Organs 23(1):114–118; 1999.

11. Leheste, J. R.; Rolinski, B.; Vorum, H.; Hilpert, J.; Nykjaer, A.; Jacobsen, C.; Aucouturier, P.; Moskaug, J. O.; Otto, A.; Christensen, E. I.; Willnow, T. E. Megalin knockout mice as an animal model of low molecular weight proteinuria. Am. J. Pathol. 155(4):1361–1370; 1999.

12. Matsumoto, K.; Nakamura, T. Hepatocyte growth factor: Renotropic role and potential therapeutics for renal diseases. Kidney Int. 59(6):2023–2038; 2001.

13. Mignon, A.; Guidotti, J. E.; Mitchell, C.; Fabre, M.; Wernet, A.; De La Coste, A.; Soubrane, O.; Gilgenkrantz, H.; Kahn, A. Selective repopulation of normal mouse liver by Fas/CD95-resistant hepatocytes. Nat. Med. 4(10):1185–1188; 1998.

14. Oertel, M.; Rosencrantz, R.; Chen, Y. Q.; Thota, P. N.; Sandhu, J. S.; Dabeva, M. D.; Pacchia, A. L.; Adelson, M. E.; Dougherty, J. P.; Shafritz, D. A. Repopulation of rat liver by fetal hepatoblasts and adult hepatocytes transduced ex vivo with lentiviral vectors. Hepatology 37(5):994–1005; 2003.

15. Seikaly, M.; Ho, P. L.; Emmett, L.; Tejani, A. The 12th Annual Report of the North American Pediatric Renal Transplant Cooperative Study: Renal transplantation from 1987 through 1998. Pediatr. Transplant. 5:215–231; 2001.

16. Suzuki, A.; Zheng, Y. Y.; Kaneko, S.; Onodera, M.; Fukao, K.; Nakauchi, H.; Taniguchi, H. Clonal identification and characterization of self-renewing pluripotent stem cells in the developing liver. J. Cell Biol. 156(1):173–184; 2002.

17. Tran, M.; Rutecki, G. W.; Sprague, S. M. The pathogenesis of beta(2)-microglobulin-induced bone lesions in dialysis-related amyloidosis. Semin. Dial. 14(2):131–133; 2001.

18. U.S. Department of Health and Human Services. Guide for the care and use of laboratory animals. NIH Publication No.85-23; Washington, DC; 1985.

Brap2 Functions as a Cytoplasmic Retention Protein for p21 during Monocyte Differentiation

Minoru Asada,[1,2]† Kazuhiro Ohmi,[3] Domenico Delia,[4] Shin Enosawa,[5] Seiichi Suzuki,[5] Akira Yuo,[2] Hidenori Suzuki,[6]† and Shuki Mizutani[1]*

Department of Pediatrics and Developmental Biology, Graduate School of Medicine, Tokyo Medical and Dental University,[1] and Department of Pharmacology, Nippon Medical School,[6] Bunkyo-ku, Department of Hematology, Research Institute, International Medical Center of Japan, Shinjuku-ku,[2] and Department of Pathology[3] and Department of Surgery,[5] National Children's Medical Research Center, Setagaya-ku, Tokyo, Japan, and Department of Experimental Oncology, Istituto Nazionale Tumori, Milan, Italy[4]

The cell cycle inhibitor p21 plays an important role in monocytic cell differentiation, during which it translocates from the nucleus to cytoplasm. This process involves the negative regulation of the p21 nuclear localization signal (NLS). Here, we sought to determine the relationship between the cytoplasmic translocation of p21 and another molecule, Brap2, a cytoplasmic protein which binds the NLS of BRCA1 and was recently reported to inactivate KSR in the Ras-activating signal pathway under the name of IMP. We report that p21 and Brap2 directly interact, both in vitro and in vivo, in a manner requiring the NLS of p21 and the C-terminal portion of Brap2. When it is cotransfected with Brap2, p21 is expressed in the cytoplasm. Monocytic differentiation of the promyelomonocytic cell lines U937 and HL60 is associated with the upregulation of Brap2 expression concomitantly with the upregulation and cytoplasmic relocalization of p21. Our results underscore the role played by Brap2 in the process of cytoplasmic translocation of p21 during monocyte differentiation.

The hormone 1,25-dihydroxyvitamin D_3 (VD_3) can induce differentiation of hematopoietic cell lines such as HL60 and U937 along a macrophage-monocyte pathway. In a search for VD_3 target genes, the cell cycle inhibitor p21 and the homeobox gene product HoxA10 were identified as direct transcriptional targets of the VD_3 receptor (15, 19). HoxA10 can directly bind to the p21 promoter, together with its trimeric partners PBX1 and MEIS1, and activate p21 transcription (5). It has been shown that VD_3-induced monocytic differentiation is associated with the initial nuclear expression and subsequent cytoplasmic translocation of p21 (3). Furthermore, we have demonstrated that peripheral blood monocytes express p21 in the cytoplasm, which appears important for their survival and for specific function. Cytoplasmic p21 expression protects monocytes by preventing the induction of the activated mitogen-activated protein kinase pathway by reactive oxygen species. This protection is accomplished in part by binding to and inhibiting ASK1, which otherwise triggers cell death.

Several tumor suppressor genes, including BRCA1, encode nuclear proteins, the functions of which are critically dependent on their correct nuclear localization. BRCA1 is normally located in the nucleus and plays important roles in DNA damage monitoring and repair (20). The mechanisms regulating the nuclear localization of BRCA1 are prerequisite to its tumor suppressor activity, and their dysregulation may lead to cellular transformation. In contrast to normal breast epithelial cells, where BRCA1 is found in the nucleus, in many advanced breast cancer cells BRCA1 is mislocated to the cytoplasmic compartment (6). In an attempt to identify the underlying mechanism for BRCA1 mislocation, Li et al. searched for proteins that interacted with the nuclear localization signal (NLS) of BRCA1 and identified Brap2 (BRCA1-associated protein 2), which is predominantly localized to the cytoplasm (13). Subsequent studies, however, failed to show any direct link between Brap2 and the intracellular localization of BRCA1. Nonetheless, Brap2 is a unique cytoplasmic protein whose properties include the ability to bind the NLS motif and, as was recently reported, to inactivate KSR, a scaffold or adaptor protein that couples activated Raf to its substrate MEK (16).

During the investigation of nuclear p21 translocation to the cytoplasm, we found that Brap2 binds p21 and, moreover, that this binding is required for the cytoplasmic localization of p21.

MATERIALS AND METHODS

Plasmids. Green fluorescent protein (GFP)-fused p21 expression vector was constructed by ligating PCR fragments of p21 with pEGFP-C2 vector (Clontech). Corresponding p21 fragments are as follows: nuclear export signal (NES)-NLS (amino acids [aa] 71 to 164), NES-dNLS (deletion of the NLS) (aa 71 to 140), dNES-NLS (aa 79 to 164), dNES-dNLS (aa 79 to 140), C-terminal NLS (aa 111 to 164), and C-terminal dNLS (aa 111 to 140). GFP-fused Brap2 expression vector was constructed by ligating full-length Brap2 amplified by PCR using differentiated U937 cDNA as a template. Myc-tagged Brap2 was constructed using pCMV-Tag1 vector (Stratagene). pCMV-Brap2 vector was also constructed using pcDNA3.1 (Invitrogen). For in vitro translation, Myc-tagged Brap2 was cloned into pBluescript-KS vector (Stratagene). C-terminal Myc-tagged full-length p21 and flag-tagged dNLS p21 (aa 1 to 140) were also constructed using PCR fragments as inserts. The glutathione S-transferase (GST) fusion system was used to generate fusion proteins. Several expression plasmids were constructed using the pGEX-5X vector (Pharmacia): GST-p21C (aa 87 to 164), GST-p21C dNLS (aa 87 to 140), and GST-p21 (aa 1 to 164). Expression of the fusion protein was induced by the addition of isopropyl-β-D-thiogalactopyr-

* Corresponding author. Mailing address: Department of Pediatrics and Developmental Biology, Graduate School of Medicine, Tokyo Medical and Dental University, 1-5-45 Yushima, Bunkyo-ku, Tokyo 113-8519, Japan. Phone: 81-3-5803-5244. Fax: 81-3-3818-7181. E-mail: smizutani.ped@tmd.ac.jp.
† Present address: Department of Pharmacology, Nippon Medical School, Bunkyo-ku, Tokyo, Japan.